Direct measurement of frequency-dependent phase velocities from snowflake data

Chioma Chineke and Kris Innanen

ABSTRACT

CCS is an effective technique for reducing or eradicating the CO2 imprint in the atmosphere. However, continuous monitoring of the sequestrated CO2 is important to make sure it remains contained within the geological storage. The data analyzed in this research is from the Newell County facility. Newell County facility is a shallow CO2 injection project which continuously encourages the development of new technologies for measurement, monitoring and verification related to CCS.

The seismic method is useful for estimating the frequency-dependent phase velocities of seismic waves. The velocity of a wave in a medium is determined by the properties of that medium and the frequency of the wave. From dispersion, we understand that seismic waves of varying frequency travel with different velocities, largely due to the non-uniform elastic properties in the subsurface. In this research, we are interested in estimating the phase velocities of the frequencies of the seismic waves as it varies along different direction of seismic propagation.

The method used in this study is concerned with the analysis of uncorrelated vibroseis data, with a focus on the frequency dependence of seismic velocities. We are concerned with the estimation of frequency-dependent phase velocities, which is largely based on exploiting the difference in the arrival and departure times of each frequency present in the data.

INTRODUCTION

Carbon dioxide is one of the greenhouse gases responsible for global warming and climate change; therefore, capturing and storing carbon dioxide is essential to protect the climate in a process called carbon sequestration. Carbon Capture and Storage (CCS) is a crucial technology for reducing greenhouse gas emissions and mitigating climate change. CCS has become increasingly important in Canada's efforts to address climate change, as it is one of the world's major emitters of greenhouse gases. To ensure the safe and effective implementation of CCS projects, it is critical to identify suitable storage facilities for sequestered CO2, and deep saline geological formations have the necessary porosity, permeability, and seal rock (Daley et. al,2019).

One such project in Alberta is the Newell County facility, a shallow CO2 sequestration experiment around 300m in depth, which aims to be the world’s leading site for testing, and supporting the development of new Measurement, Monitoring, and Verification (MMV) technologies related to geological CO2 sequestration. The Containment and Monitoring Institute (CaMI) operates this field research station in collaboration with the University of Calgary. The injection interval at the facility is the Basal Belly River Sandstone (BBRS), a brine-saturated reservoir of 10% porosity at the base of the Foremost Fm (Dongas, 2016, Macquet and Lawton, 2017).

To ensure the permanent containment of sequestered CO2 within the geological formation without leakage, monitoring the sequestered CO2 at the injection stage and throughout all stages of the CCS projects (Thomas M. Daley et. al,2019). The seismic method is a useful tool for monitoring fluid movement within the subsurface, as the injection of CO2 into the geological formation causes changes in the elastic and acoustic properties of the propagating waves within the geological storage, as described by Gassmann F. 1951.

Analyzing data from the Newell County facility, although a shallow CO2 injection project would strongly improve the understanding of how seismic data behave in the near-surface since it is fundamental to efficient seismic interpretation at deeper targets.

The method used in this study is concerned with the analysis of uncorrelated vibroseis data, with a focus on the frequency dependence of seismic velocities. This approach was initially proposed by Dragoset in a maritime context in 1988. In subsequent years, Sun and Milkereit (2007) and Sun et al. (2009) expanded upon this concept by using the sensitivity to analyze proper body wave dispersion and developing a VSP data correlation scheme. In 2010, Haase utilized this method to model VSP data, using velocity and density logs. Kris et al., 2014 utilized a multicomponent walkaway VSP data set to estimate dispersion.

In this study, we are concerned with the estimation of frequency-dependent phase velocities, which is largely based on exploiting the difference in the arrival and departure times of each frequency present in the data, while understanding that high-frequency waves travel with higher velocities than lower-frequency waves, but the vibroseis sweep favours the earlier release of the lower frequencies over that of the higher frequencies, Aki and Richards (2002).

THEORY

In vibroseis seismic surveys, the lowest frequencies are typically input first into the earth because they are better able to penetrate deeper into the subsurface and provide information about deeper geological structures. The higher-frequency sweeps, which are used to image shallower structures with higher resolution, are sent in a bit later. However, Aki and Richards (2002) dispersion models of body waves predict that higher seismic frequencies propagate more quickly than lower seismic frequencies. In a dispersive medium, these high frequencies propagate with a higher phase velocity than the low frequencies in a bid to catch up with the lower frequencies (Kris Innanen, et al. 2014). This means that the source delays the input of higher frequencies into the medium (dispersive), but when it eventually does, the dispersive medium propels the higher frequencies forward. Kris Innanen et al (2014) describe in detail the analysis and mathematical explanation of estimating dispersion from uncorrelated VSP data.

METHODS

Data set

A walkaway VSP is the seismic technique employed in the acquisition of the data used in this study. The seismic source used in the acquisition is the vibroseis linear sweep. A sweep is a signal that is transmitted into the ground during a seismic survey and consists of a variety of frequencies. This sweep signal generates seismic waves of various frequencies, which propagate into the subsurface and interact with geologic layers and structures. The recording sensors were the 3-component accelerometers.

The acquisition geometry for the walk-away VSP dataset is illustrated in Figure 1. There are twelve shot lines with the injection well at the center. The accelerometers are aligned 1m apart along the observation well. This analysis focused on the vertical and horizontal component linear sweep vibroseis data, allowing for the observation of individual frequency components and their travel times to identify dispersion effects.

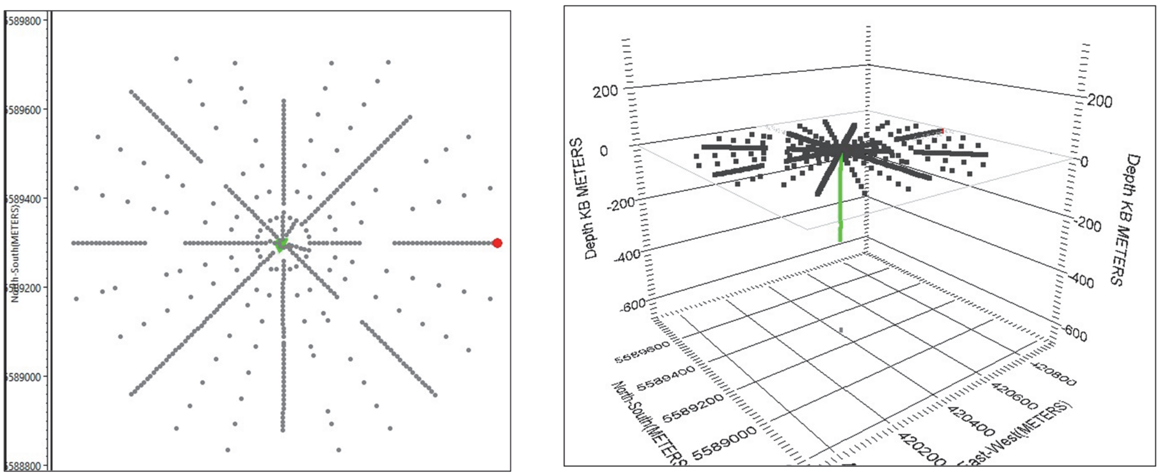

Figure 1: Acquisition geometry made up of 12 shot lines with the receivers aligned 1m apart along the observation well.

Phase velocity

In this research, we are interested in estimating the phase velocity of the frequency present in the data. The phase velocity is the ratio of the propagating distance of the direct P-wave to the travel time of a particular frequency.

The propagation distance is the square root of the sum of squares of the location of the shot and the receiver, with the assumption of a straight ray path.

The travel time of frequency, f is the difference between the time it takes the frequency f to arrive at the receiver and the time it takes it to depart from the source.

The departure time of seismic wave with frequency from the sweep

At the time, t=0 which marks the beginning of the vibroseis sweep program. A typical mathematical representation of the sweep program is expressed as:

$$S(t) = Im[a(t)e^{i\emptyset(t)}] \qquad (1)$$

The amplitude function, $a(t)$ decreases as time moves away from the centre of the function (exhibits a tapering effect during the early and late times) while the phase is defined as:

$$\emptyset(t) = 2\pi f(t)t \quad (2)$$

The equation shows that frequency is time-dependent, and that phase is a function of time-dependent frequency.

The linear sweep can be mathematically represented as:

$$f(t) = fmin + \frac{(fmax - fmin)t}{T} \quad (4)$$

where $fmin$ and $fmax$ are the low and high-frequency limits respectively while T is the sweep length. The time, $T_s(f)$ at which the frequency f departs the vibroseis sweep is the inverse of $f(t)$.

$$T_s(f) = \frac{f - fmin}{fmax - fmin}T \quad (5)$$

The propagation time of a seismic wave of frequency f within the medium.

The time, $\Delta T(f)$ it takes the seismic signal at frequency f to travel from the source to the geophone depends on the path taken within the subsurface medium and the propagation velocity of the wave. We assume that the seismic waves travel in a straight line between the source and the receiver (straight ray path) in this study:

$$\Delta T(f)^2 = \frac{x_s^2 + z_g^2}{C(f)^2} \quad (6)$$

Arrival time of seismic wave with frequency f at the geophone.

Time, $T_M(f)$ at which the seismic wave with frequency f arrives at the accelerometer after travelling through an assumed straight ray path of distance $L = (x_s^2 + z_g^2)^{1/2}$ is:

$$T_M(f) = T_s(f) + \frac{L}{C(f)} \quad (7)$$

The dispersive phase velocity, $C(f)$ of the seismic wave can thus be calculated by the relationship:

$$C(f) = \frac{L}{T_M(f) - T_s(f)} \quad (8)$$

Where L is estimated from the assumption of a straight ray path between source location, x_s^2 and geophone depth, z_g^2. When the Gabor transform of the sweep is superimposed on that of the uncorrelated vibroseis record, with the frequency $fmin$ set at time =0, the change in time $T_M(f) - T_s(f)$ can be picked.

Time-frequency decomposition of the vibroseis response

The Gabor transform is a time-frequency analysis technique used to decompose a signal into its frequency and time components.

Gabor transform is a mathematical function transformation that yields a combined time-frequency representation of a given signal and a method to extract the signal from this time-frequency representation. The Gabor transform $G\,f(t,w)$ of a given signal $f(t)$ identifies the spectral strength energy present in the signal close to time t at frequency, w as a function of two variables.

$$G\,f(t,w) = \int_{-\infty}^{\infty} f(s)g(s-t)e^{-2\pi isw}\,ds \tag{9}$$

This mathematical representation of Gabor transform could be thought of as Fourier transforms within a time window, where $g(s-t)$ is the window function (Lamoureux et al, 2003).

In this research, the time-frequency decomposition of the traces and sweep was generated using the Gabor transform. The arrival and departure time of any given frequency was estimated from the time-frequency decomposition plots.

Picking of first breaks

By analyzing the Gabor transform results, the departure time of each frequency from the sweep can be manually picked. This involves identifying the time at which each frequency component becomes dominant in the signal and separates from the other components. The departure time is the time at which the seismic wave corresponding to a specific frequency is generated or emitted during the sweep.

Similarly, the frequency arrival time at the accelerometer can be manually selected from the Gabor transform results. This entails determining the time when a seismic wave of a given frequency arrives at the accelerometer.

It is feasible to estimate the travel duration of the seismic wave between the source and the accelerometer for each frequency by selecting the departure and arrival times for each frequency component.

Dispersion Estimation

The time difference between when a certain frequency leaves the programmed sweep and when it arrives at the accelerometer is referred to as the "travel time" or "time delay" of the seismic wave for that frequency. This is the time it takes for the wave to propagate through the subsurface from the source to the accelerometer.

The travel time of the seismic wave for each frequency is used as input in the calculation to determine the dispersive wave velocity in equation (7).

Estimation of the uncalibrated (raw) phase velocity

Using the equation 8, we could estimate the phase velocity, which is the ratio of the radial distance to the travel time of each frequency. The phase velocity estimated at this stage is the uncalibrated or raw phase velocity.

Calibration of phase velocity

The arrival and departure time picks were picked with high accuracy but were exposed to a constant error. To account for this error, calibration time, Tcal is introduced from the group velocity of the direct P wave from the near offset shot record.

$$C(f) = \frac{L}{T_M(f) - T_S(f) - \mathrm{T(cal)}} \quad (9)$$

RESULTS

Uncorrelated seismic traces at different receivers were extracted for a shot record and plotted in figure 2 as amplitude variation with time.

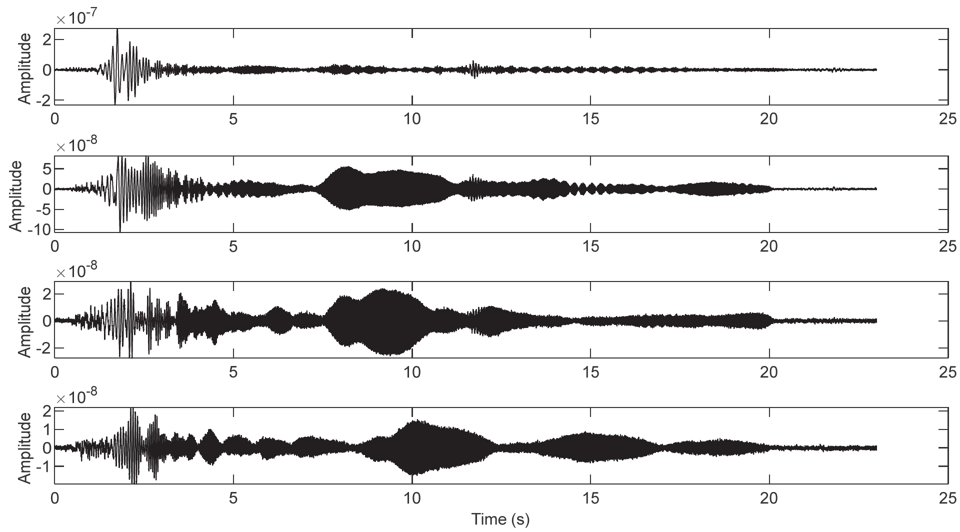

. Figure 2: Uncorrelated seismic traces for a shot record extracted at different receiver depths.

The source signal was estimated using equations 1-4. It is plotted as amplitude variation with time in Figure 3.

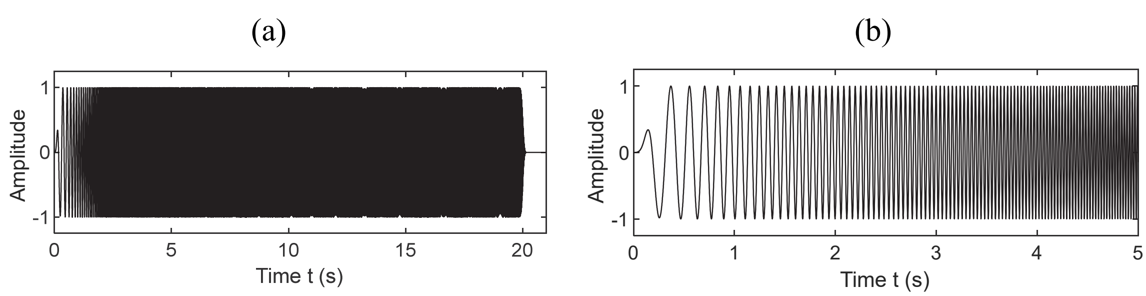

Figure 3a: Estimated source signal plotted as amplitude variation with time ;(3b) Plot of the first 5s of the source signal.

Estimating the travel time of the frequencies is an essential step in calculating the phase velocities, the source signal and seismic traces need to be transformed from time domain to frequency domain. This was done using the Gabor transform code from CREWES toolbox. The Gabor spectrum from a transformed seismic trace in figure 4 contains different labelled events. The event that contains the information of interest, in this research is the event labelled vibroseis sweep.

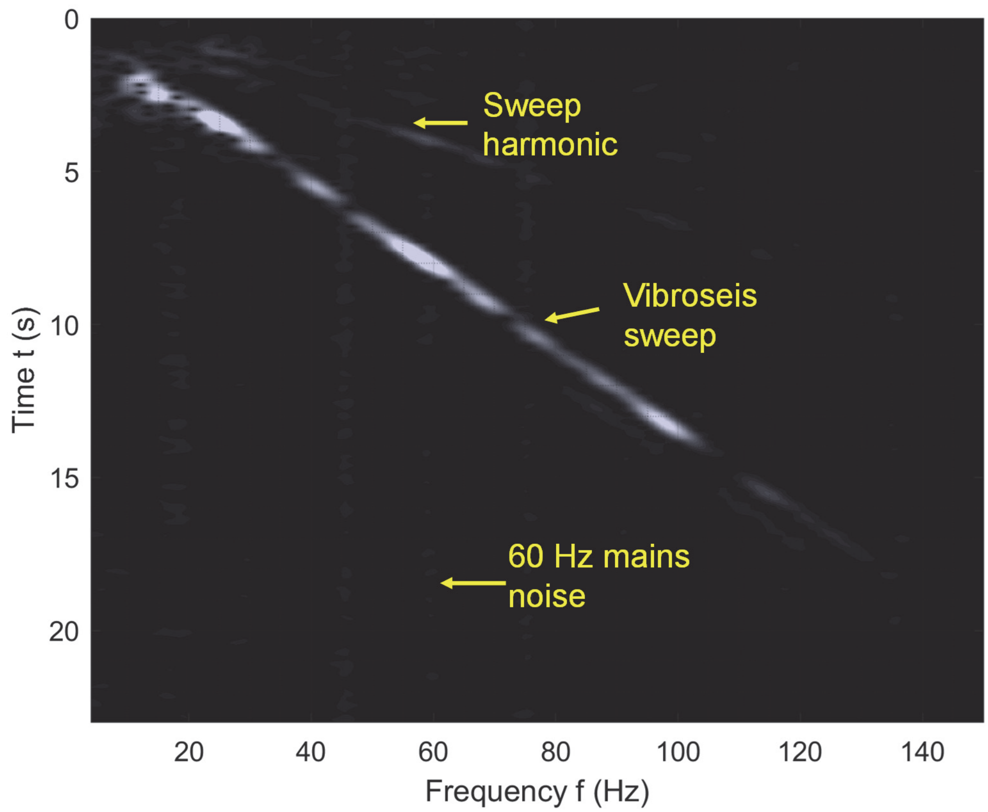

Figure 4: Gabor Transform of an uncorrelated seismic trace with different events labelled.

The Picking of the arrival time and departure times in figures 5 and 6 were done using a semi-automatic picking approach. An assumption that the estimated time for each frequency smoothly deviates from the linear was followed. The arrival and departure time picks were picked for about 13 frequencies, and these were fitted with a 5^{th} order polynomial. This polynomial enhanced the interpolation of the times picks within frequency intervals.

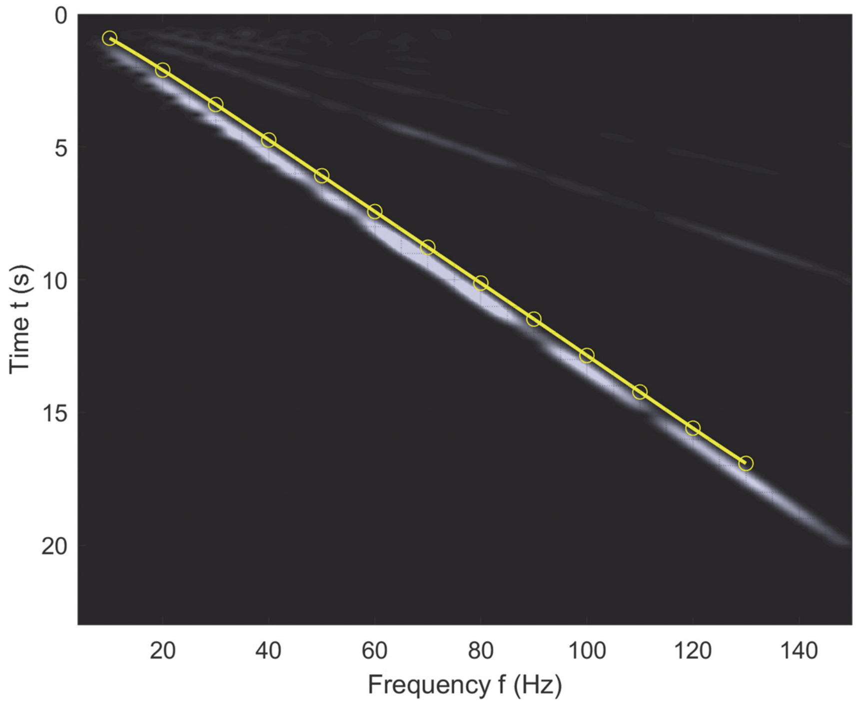

Figure 5: Picking of arrival times of the frequencies on an Gabor spectrum of the uncorrelated seismic trace.

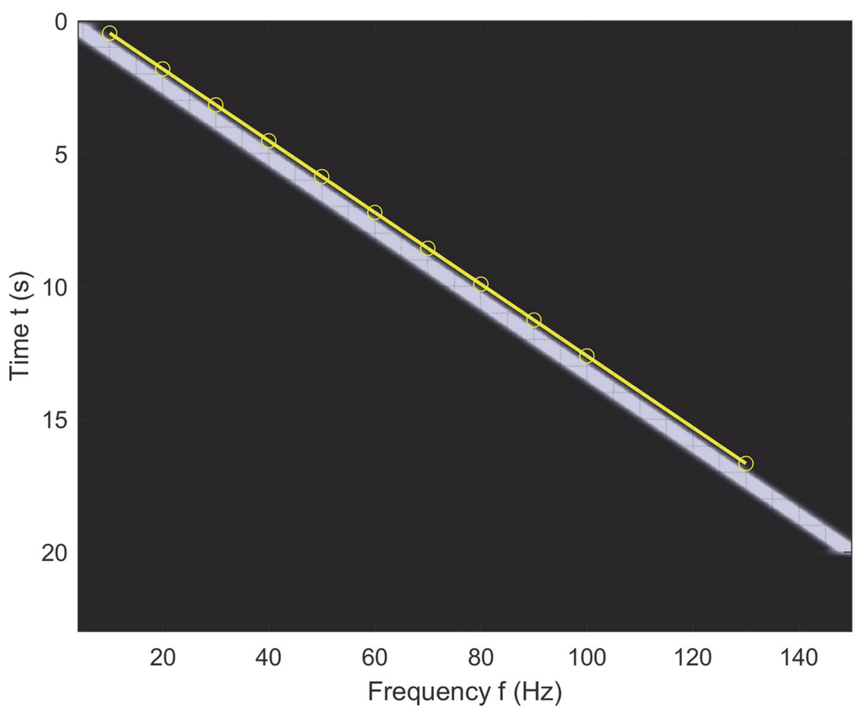

Figure 6: Picking the departure times of the frequencies from the Gabor spectrum of the signal.

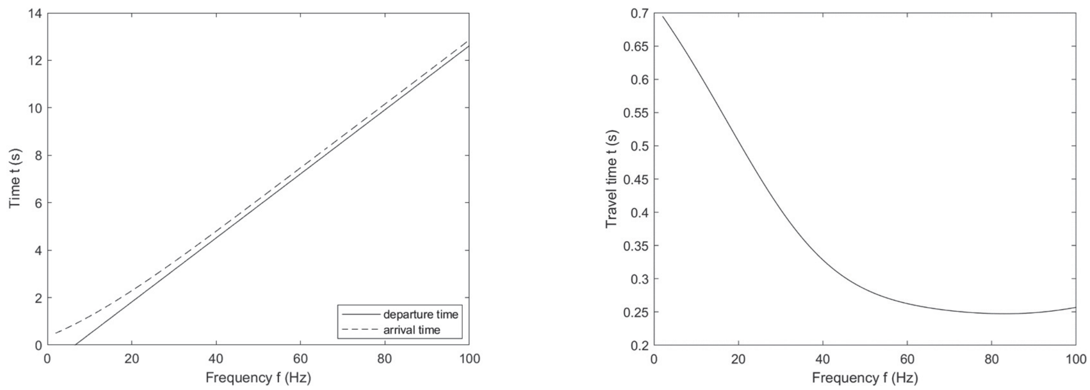

Figure 7a: A plot of the overlay of both the departure time and the arrival times; (7b) A plot of the travel time of the frequencies.

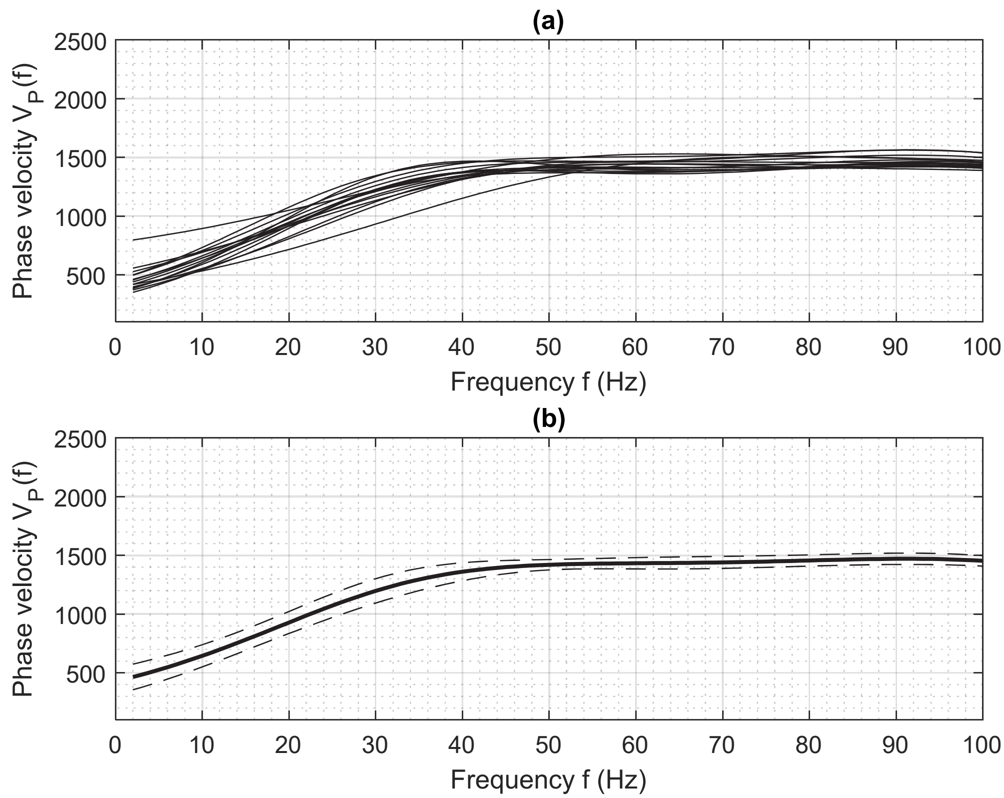

Figure 8a: Uncalibrated phase velocities estimated from seismic traces between depths 3 – 150m; (8b) A plot of the mean value of the phase velocities in 8a.

A plot travel time, figure 7 of the frequencies in figure 5 shows the difference between the departure and arrival times for each frequency component of the seismic wave.

Dividing the radial distance by the travel time of each frequency using equation (6) would yield the uncalibrated (raw) phase velocity. The arrival and departure times were affected by a constant error, despite the high accuracy employed while picking the times.

From the understanding that seismic waves of varying frequencies travel with different velocities and this is predominant at low frequencies (2-40 Hz) and at a dominant frequency, the seismic waves start travelling with the same group velocity.

Tcal estimated in figure 9 with respect to the group velocity is applied to the uncalibrated phase velocities in figure 8 to nullify the constant error and produce calibrated phase velocities in figure 10.

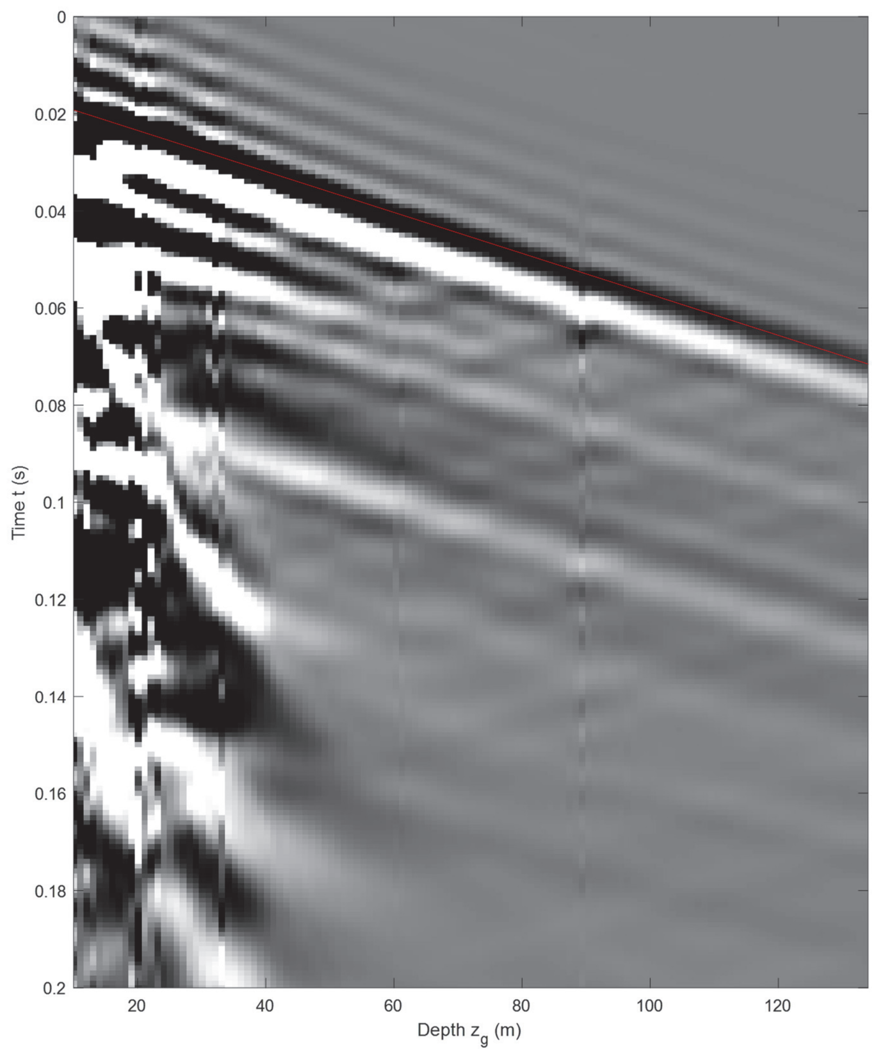

Figure 9: Calculation of group velocity used in estimating Tcal required for calibrating the raw phase velocities.

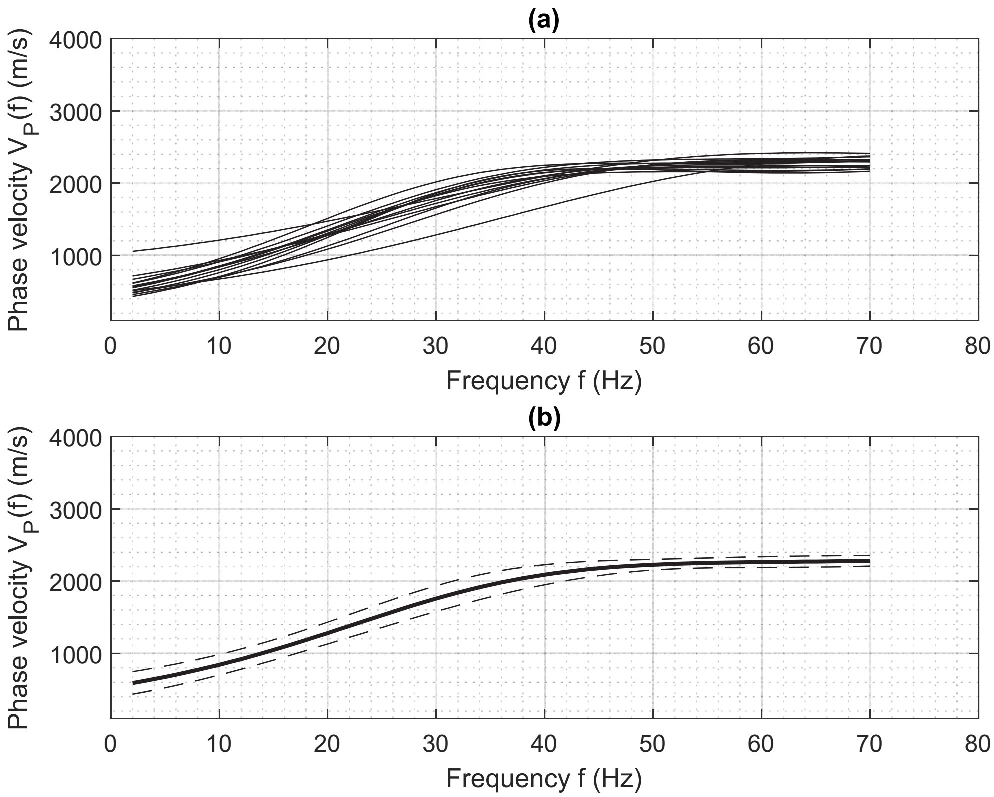

Figure 10a: A plot of the calibrated phase velocities estimated at depths 3-150m; (10b) A plot of the mean of the estimated calibrated phase velocities.

The estimation of phase velocities was carried out for shot records at along different shot lines and at varying offsets for seismic traces at different receiver depths. Figures 11 and 12 are maps showing the variation of phase velocities along offsets and along different directions of seismic propation.

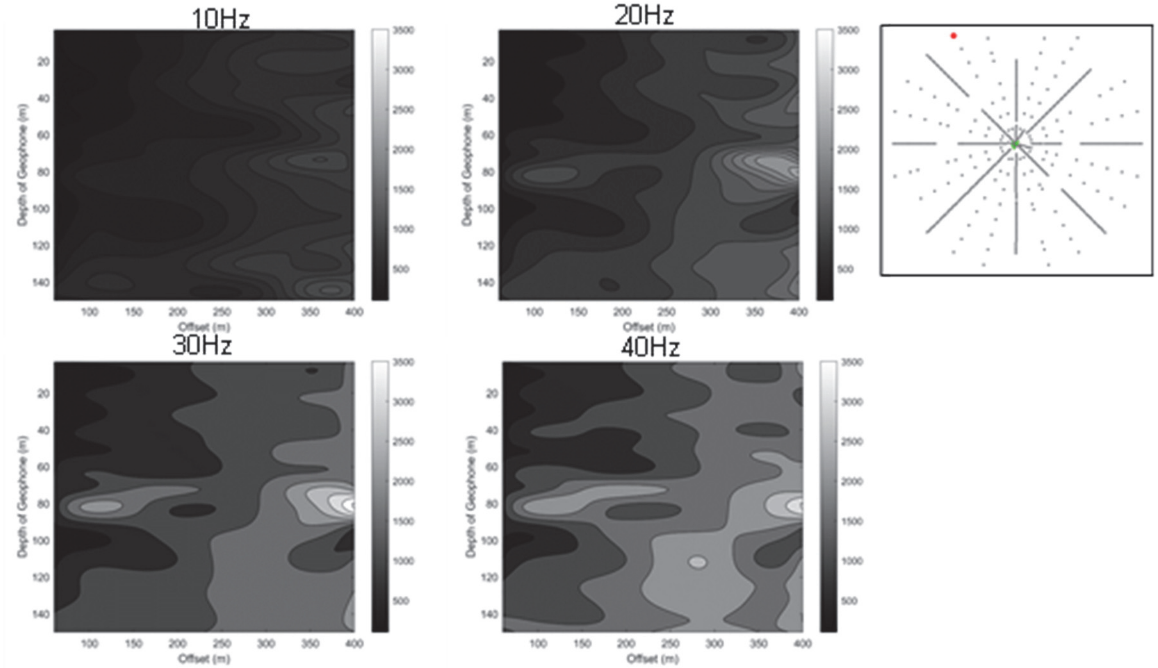

Figure 11: Maps of estimated phase velocities along the same offsets at varying frequencies along line 9

(a)

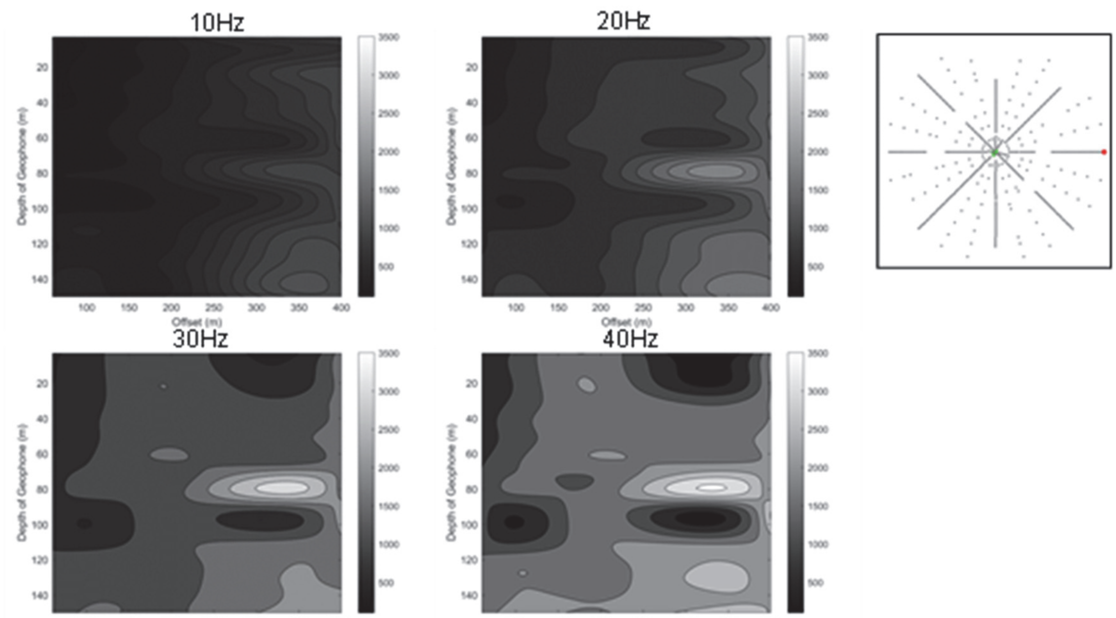

Figure 12a: Maps of estimated phase velocities along the same offsets at varying frequencies, along Line 1(10-40hz); (12b) Maps of estimated phase velocities along the same offsets at varying frequencies , along Line 4.

(b)

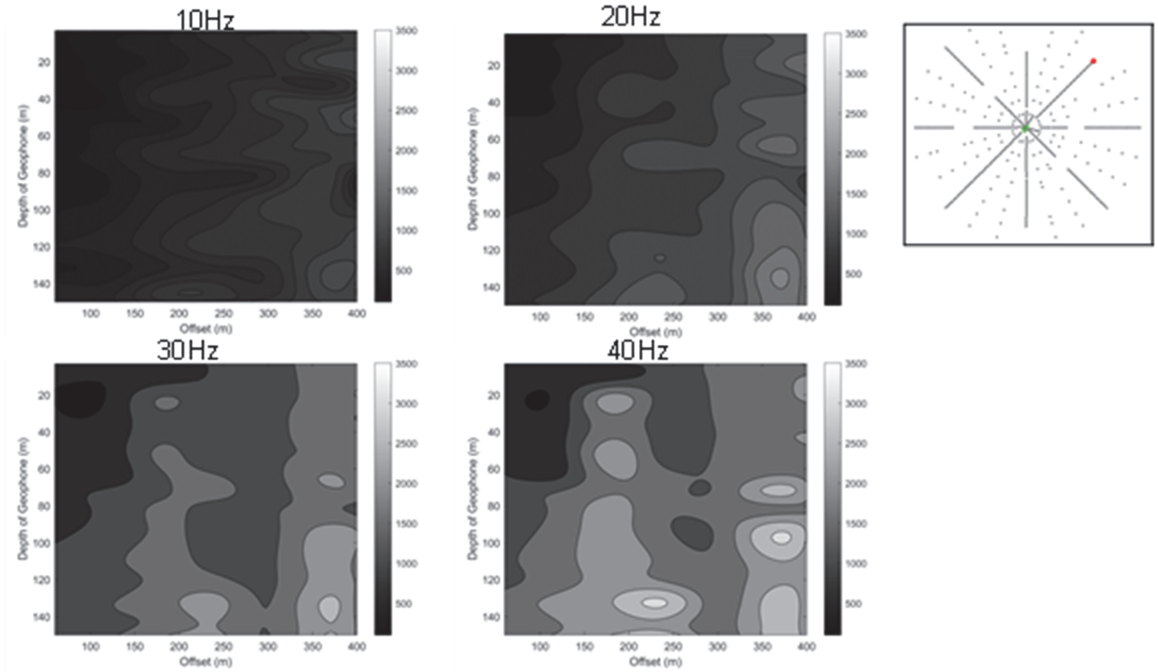

Figure 12b: Maps of estimated phase velocities along the same offsets at varying frequencies, along Line 1(10-40hz); (12b) Maps of estimated phase velocities along the same offsets at varying frequencies , along Line 4.

Semi-automatic or manual picking of the arrival times and departure times could be time consuming, although quite effective. An automatic picking code developed by Joe Wong et al., that uses the modified energy ratio (MER) to pick first arrival in figure 13 a and b was used to pick both the arrival and departure time of the frequencies. Refer to Joe Wong's CREWES report on MER for better understanding of how MER works.

(a) (b)

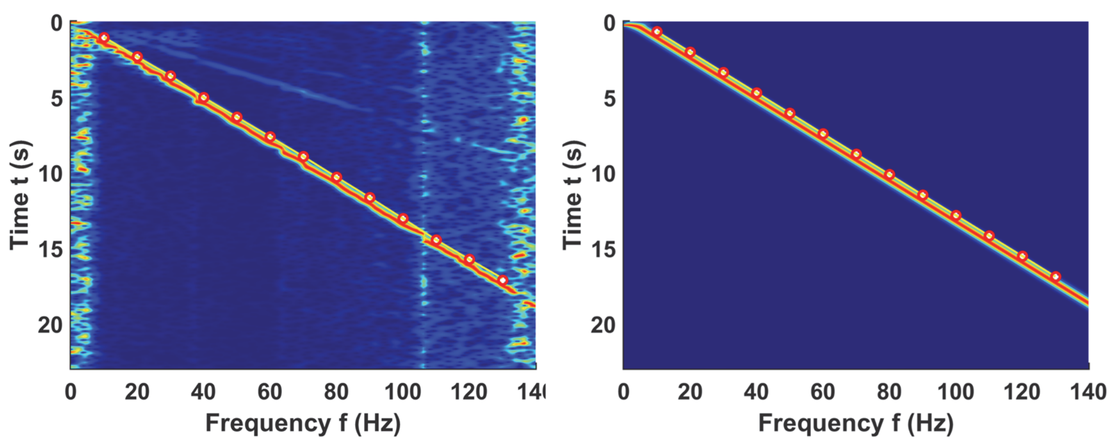

Figure 13a: Automatic picking of the arrival times of the frequencies; (13b) Automatic picking of the departure times of the frequencies.

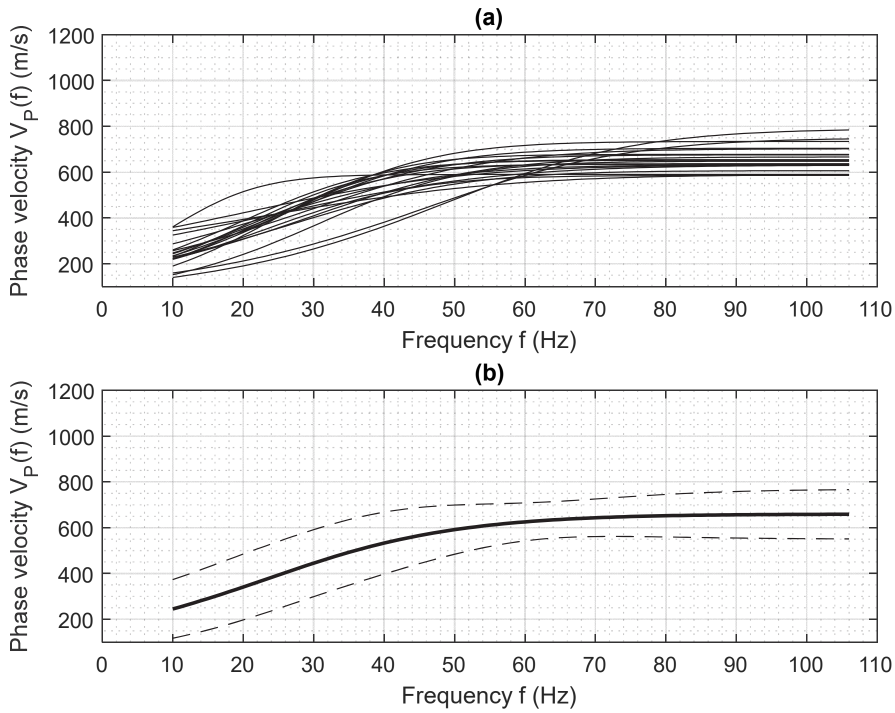

Figure 14a: A plot of the uncalibrated phase velocities estimated at depths 3-232m;(14b) A plot of the mean of the estimated uncalibrated phase velocities.

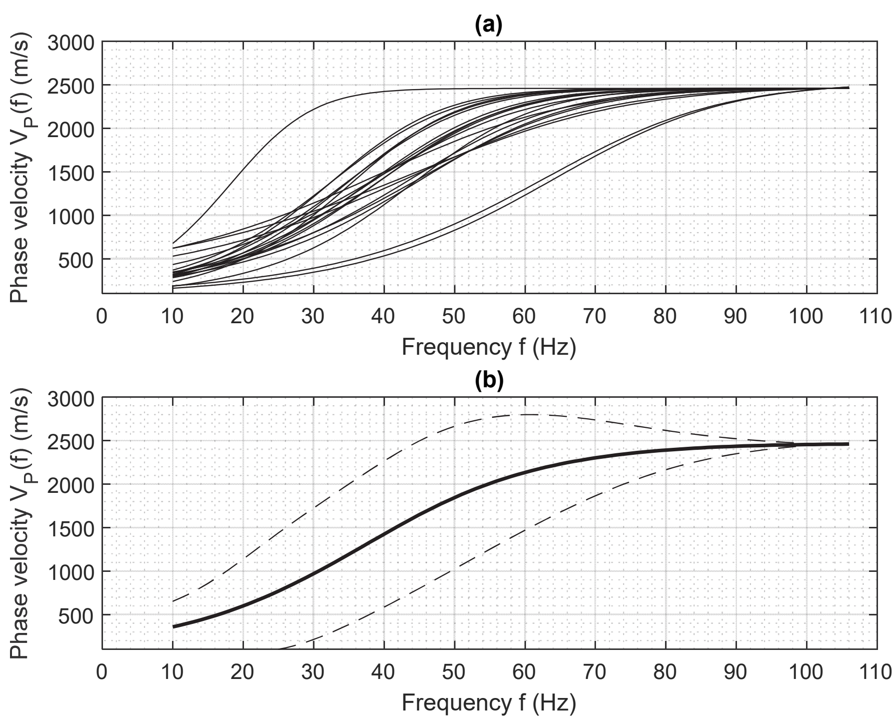

Figure 15a: A plot of the calibrated phase velocities estimated at depths 3-232m;(14b) A plot of the mean of the estimated calibrated phase velocities.

The uncalibrated phase velocities in figure 14 estimated were also calibrated to nullify the effect of the inherent constant error it was exposed to. This produced the calibrated phase velocities in figure 15.

Maps in figure 16 depicts the variation of phase velocities along lines 1 at different offsets.

SUMMARY

Analyzing the VSP datasets from the Newell County facility would help enhance the understanding of seismic data in the near-surface.

Seismic waves of varying frequencies travel with different velocities (phase velocities) largely because of the non-uniformity of the elastic property in the subsurface, this is predominantly obvious within the low frequencies, at dominant frequencies the seismic waves start to travel with little or no variation in their velocities (group velocities).

Seismic phase velocity is a function of frequency and the elastic property of rocks, which could be calculated by finding the ratio of the propagation distance of the direct P-wave and the travel time of a particular frequency.

Seismic phase velocity varies with offsets and along different directions of wave propagation.

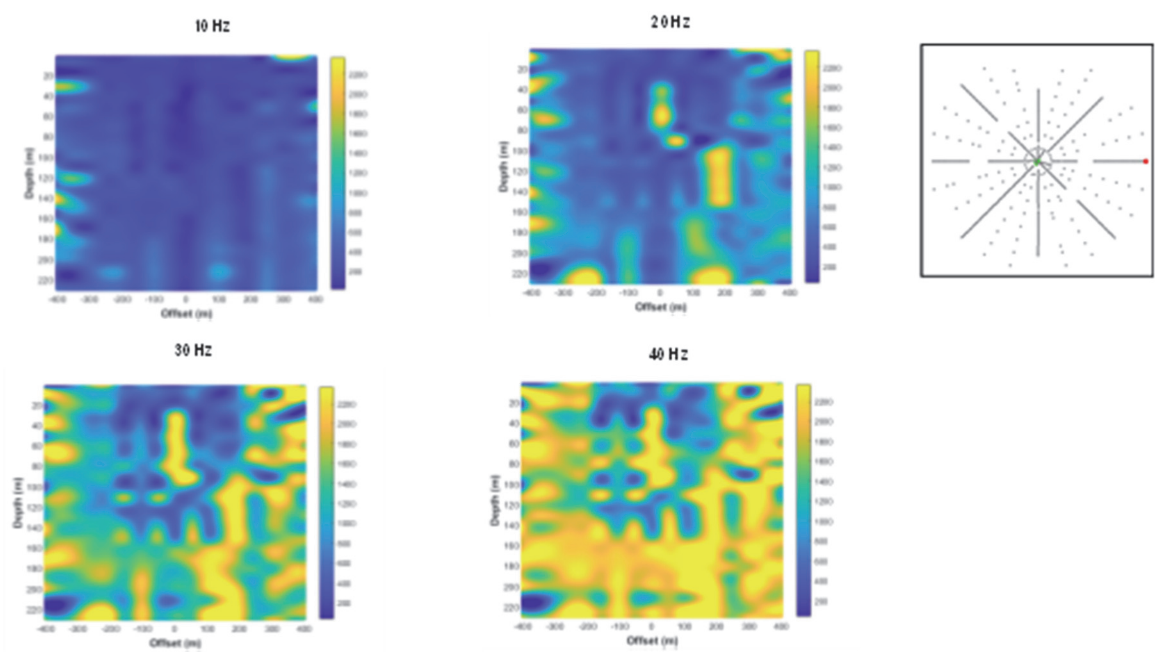

Figure 16: Maps of estimated phase velocities along the same offsets at varying frequencies (10-40Hz), along Line 1.

ACKNOWLEDGEMENTS

The sponsors of CREWES are gratefully thanked for continued support. This work was funded by CREWES industrial sponsors, NSERC (Natural Science and Engineering Research Council of Canada) through the grant CRDPJ 543578-19. This work was done in collaboration with the Carbon Management Canada.

REFERENCES

Aki, K., and Richards, P. G., 2002, Quantitative Seismology: University Science Books, 2nd edition.

Cheng, P., 2013, Anelastic attenuation in seismic data: modelling, measurement, and correction: Ph.D. thesis, The University of Calgary.

Daley, T., & Harbert, W. (2019). Goals of CO2 Monitoring: Why and How to Assess the Subsurface Changes Associated with Carbon Capture and Storage. In T. Davis, M. Landrø, & M. Wilson (Eds.), *Geophysics and Geosequestration* (pp. 54-70). Cambridge: Cambridge University Press. doi:10.1017/9781316480724.004

F. Gassmann, "Uber die Elastizitat Poroser Medien," Veirteljahrsschrift der Naturforschenden Gesellschaft in Zzirich, Vol. 96, 1951, pp. 1-23

Hall, K. W., Lawton, D. C., Holloway, D. E., and Gallant, E. V., 2012, Husky 2011 walkaway 3C-VSP: CREWES Annual Reports, 24.

Kris Innanen, 2014, Estimating anelastic dispersion from uncorrelated vibe data, vol 16: CREWES Reports

Macquet, M., Lawton, D. C., Saeedfar, A. A., and Osadetz, K. G., 2019, A feasibility study for detection thresholds of CO_2 at shallow depths at the CaMI Field Research Station, Newell County, Alberta, Canada: *Petroleum Geoscience*, 25, no. 4., 509-518.

Margrave, G. F. and Lamoureux, M. P., 2002, Gabor deconvolution: CREWES Annual Research Report, 13.

McDonal F. J., F. A. Angona, R. L. Mills, R. L. Sengbush, R. G. Van Nostrand, and J. E. White, 1958, Attenuation of shear and compressional waves in Pierre shale: Geophysics, 23, 421-439.

Sun LF, Milkereit B, Tisato N. Analysis of velocity dispersion using full-waveform multichannel sonic logging data: A case study. Geophysical Prospecting. 2016 Jun 28;64(4):1016-29.

Wong, J., Han, L., and Bancroft, J.C., 2009. Time picking and random noise reduction on microseismic data: CREWES Report, vol. 21